IUCrJ
ISSN 2052-2525
MATERIALS | COMPUTATION

Crystal structure and magnetism in the S = 1/2 spin dimer compound $NaCu_2VP_2O_{10}$

Daisuke Urushihara,[a]* Sota Kawaguchi,[a] Koichiro Fukuda[a] and Toru Asaka[a,b]

[a]Division of Advanced Ceramics, Nagoya Institute of Technology, Nagoya 466-8555, Japan, and [b]Frontier Research Institute for Materials Science, Nagoya Institute of Technology, Nagoya 466-8555, Japan. *Correspondence e-mail: urushihara.daisuke@nitech.ac.jp

Received 3 February 2020
Accepted 22 April 2020

Edited by A. Fitch, ESRF, France

Keywords: single-crystal X-ray diffraction; electron diffraction; spin dimer compounds; magnetic susceptibility.

CCDC reference: 1976933

Supporting information: this article has supporting information at www.iucrj.org

The crystal structure of the spin dimer magnet $NaCu_2VP_2O_{10}$ was determined using single-crystal X-ray diffraction and electron diffraction. $NaCu_2VP_2O_{10}$ displayed a non-centrosymmetric orthorhombic $C222_1$ structure with a = 6.13860 (10) Å, b = 14.4846 (3) Å and c = 8.2392 (2) Å. The layered structure comprised CuO_4 plaquettes, VO_6 octahedra and PO_4 tetrahedra. A pair of CuO_4 plaquettes formed Cu_2O_6 structural dimers through edge sharing. The Cu–Cu network formed a distorted puckered-layer structure with pseudo-one-dimensional characteristics. Maximum magnetic susceptibility was observed at ~60 K and $NaCu_2VP_2O_{10}$ became non-magnetic upon further cooling. The spin gap between the spin-singlet non-magnetic ground state and triplet excited state was estimated to be 43.4 K. Thus, $NaCu_2VP_2O_{10}$ was assumed to be an alternating chain system with a singlet ground state of dimer origin. The V^{5+} ions in the VO_6 octahedra showed large off-centre displacements along the [110] direction in the primitive perovskite structure, which were attributed to the pseudo-Jahn–Teller distortion of d^0 transition metals.

1. Introduction

Quantum-spin systems have attracted considerable attention since the discovery of characteristic quantum phenomena such as superconductivity and quantum-spin liquids (Lee, 2008; Balents, 2010). Spin dimer systems are representative materials that exhibit quantum-spin fluctuations. In such systems, magnetic ions are often coupled with antiferromagnetic exchange interactions, resulting in the formation of spin dimers. Dimers are coupled with neighbouring dimers via weak exchange interactions. With increasing interactions between dimers in low-dimensional systems, spin dimer compounds can be considered as an alternating chain system. Dimerized quantum magnets usually display an energy gap between spin-singlet non-magnetic ground and triplet excited states; furthermore, the inter- and intra-dimer interactions caused by the arrangement of magnetic ions affect the energy gap.

In the spin dimer system of Cu^{2+} (S = 1/2), dimerized Cu^{2+} often shows characteristic atomic arrangements; Cu^{2+}, which possesses a $3d^9$ configuration, exhibits Jahn–Teller distortion owing to the occupied d_{3z2-r2} orbital and sometimes forms a CuO_4 plaquette or distorted CuO_6 octahedron. A CuO_4 plaquette is two-dimensional because its ligands prefer planar coordination. Thus, Cu_2O_6 dimers formed by edge-sharing CuO_4 plaquettes show various arrangements which are related to interactions between Cu ions. These Cu_2O_6 dimers have been identified in compounds such as $SrCu_2(BO_3)_2$ (Smith & Keszler, 1991; Kageyama *et al.*, 1999), $Cu_2P_2O_7$ (Effenberger,

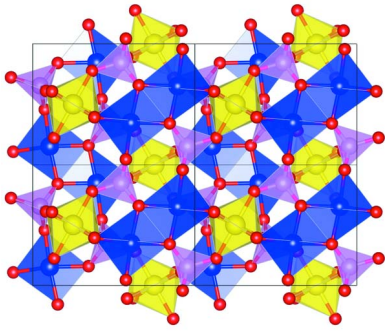

1990; Janson *et al.*, 2011) and $BaCu_2V_2O_8$ (Vogt & Müller-Buschbaum, 1990; Klyushina *et al.*, 2016). $SrCu_2(BO_3)_2$ represents a typical two-dimensional orthogonal dimer system. In $SrCu_2(BO_3)_2$, Cu_2O_6 dimers are located orthogonally along the [110] direction in a tetragonal system and connected through BO_3 triangles. In $Cu_2P_2O_7$, Cu_2O_6 dimers are located parallel to the *b* axis in the monoclinic system. The Cu–Cu network in $Cu_2P_2O_7$ has a distorted two-dimensional honeycomb structure. In contrast, $BaCu_2V_2O_8$ has three-dimensional arrangements of Cu_2O_6 dimers and its Cu–Cu network adopts pseudo-one-dimensional screw chains along the *c* axis. Both arrangements of Cu_2O_6 dimers and Cu–Cu networks strongly affect quantum states. Thus, it is important to discover other examples of spin dimer systems with a finite spin gap to an excited state.

In this study, we synthesize the spin dimer compound $NaCu_2VP_2O_{10}$, the crystal structure of which was determined using single-crystal X-ray diffraction (XRD) and electron diffraction. The obtained crystal structure is layered, and it comprises corner-sharing Cu_2O_6 dimers, VO_6 octahedra and PO_4 tetrahedra. Magnetic susceptibility measurements of $NaCu_2VP_2O_{10}$ reveal that it exhibits a non-magnetic ground state and a spin gap between the ground and excited states. We clarify that $NaCu_2VP_2O_{10}$ is an alternating chain system and discuss the relationship between its crystal structure and magnetic properties.

2. Experimental section

2.1. Synthesis

Polycrystalline samples were synthesized by a solid-state reaction. A mixture of equal amounts of $NaVO_3$ and $Cu_2P_2O_7$ was sintered at 823 K for 20 h and then 923 K for 10 h. To grow single crystals, the sintered sample was heated at 1023 K for 2 h and then cooled to 923 K at a rate of 1 K/ h. The obtained crystals had a columnar shape with a diameter of ∼50 µm.

2.2. Electron-probe microanalysis

The chemical composition of the polycrystalline materials was measured using an electron-probe microanalyzer (JXA-8230, JEOL). The prepared samples were polished to form flat surfaces. The normalized Na:Cu:V:P ratio for the three grains was determined to be 0.87 (12):2.014 (7):1.094 (3):2.022 (9), which is close to the stoichiometric chemical composition (Na:Cu:V:P ratio of 1:2:1:2).

2.3. Powder X-ray diffraction

To determine the phase purity and estimate the basic structure of the synthesized compounds, we collected powder XRD patterns using a powder X-ray diffractometer (X'Pert Pro Alpha-1, Panalytial) equipped with a high-speed detector and Cu $K\alpha_1$ X-ray source (45 kV, 40 mA). The scanning range of diffraction angles (2θ) was 5–145°, which was adequate for indexing the diffraction peaks. We confirmed that the samples did not contain any impurity phases by comparing the measured powder XRD patterns with a simulated pattern of the refined structure model of $NaCu_2VP_2O_{10}$ (see Fig. S1 in the Supporting information).

2.4. Electron diffraction

Selected-area electron diffraction (SAED) measurements were performed using a transmission electron microscope (JEM-ARM200F, JEOL) operated at 200 kV. The specimen was prepared by crushing the polycrystals; the particles were deposited on a copper grid with a holey carbon support film. We determined the space group by testing the extinction rules of the sample using SAED.

2.5. Single-crystal X-ray diffraction

Diffraction data were collected using a single-crystal X-ray diffractometer (D8 VENTURE, Bruker) equipped with a complementary metal oxide semiconductor detector and Mo $K\alpha$ X-ray source (50 kV, 1 mA). A single crystal with a diameter of ∼50 µm was mounted on a borosilicate glass needle using an adhesive. Lattice constants were determined using the *SAINT* program (Bruker, 2015) and multi-scan absorption correction was carried out using the *SADABS* program (Bruker, 2015). The initial structure model was calculated using the *SUPERFLIP* program based on the charge-flipping algorithm (Palatinus & Chapuis, 2007). Crystal structure analysis was carried out using the *JANA2006* program package (Petricek *et al.*, 2014) and the analysed crystal structure was visualized using the *VESTA* program (Momma & Izumi, 2011).

2.6. Magnetic susceptibility

The magnetic susceptibility of the polycrystalline materials was measured using a superconducting quantum-interference device magnetometer (MPMS, Quantum Design). Magnetization was obtained at 2–400 K in an applied field of 1 T.

2.7. Thermal analysis

The heat capacity of the polycrystalline materials was measured using a physical property measurement system (PPMS, Quantum Design). The temperature dependence of the heat capacity was measured at 2–300 K using a thermal-relaxation method. No thermal anomalies were observed in the investigated temperature range.

3. Results

3.1. Space group determination

We measured the powder XRD pattern of $NaCu_2VP_2O_{10}$, which could be indexed to an orthorhombic unit cell. According to the indices obtained from the powder XRD patterns, the zone axes of the incident electron beams were identified in the SAED patterns. Fig. 1 shows the SAED patterns collected under several electron beams with different incidences. In the [100] and [010] zone axis SAED patterns [Figs. 1(*a*) and 1(*b*)], only diffraction spots with indices of k =

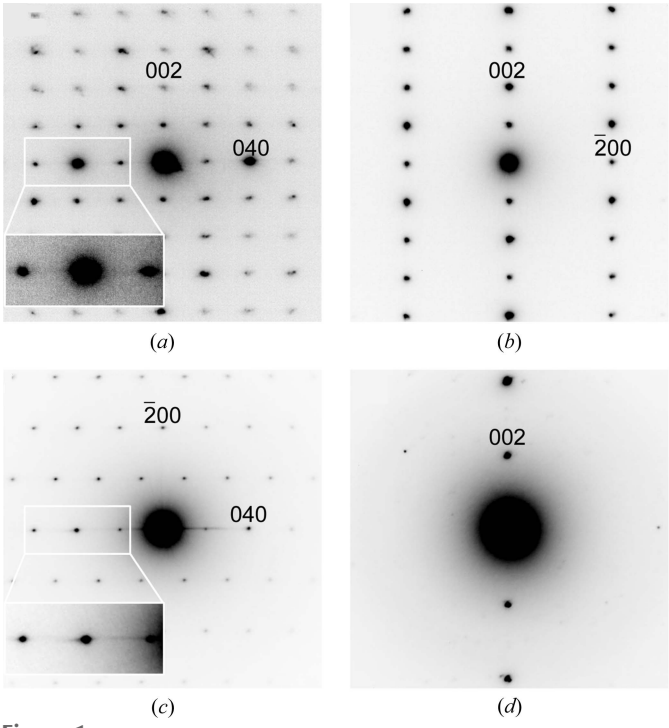

Figure 1
(*a*) [100] zone axis, (*b*) [010] zone axis and (*c*) [001] zone axis SAED patterns of $NaCu_2VP_2O_{10}$. (*d*) 00*l* systematic reflections of $NaCu_2VP_2O_{10}$.

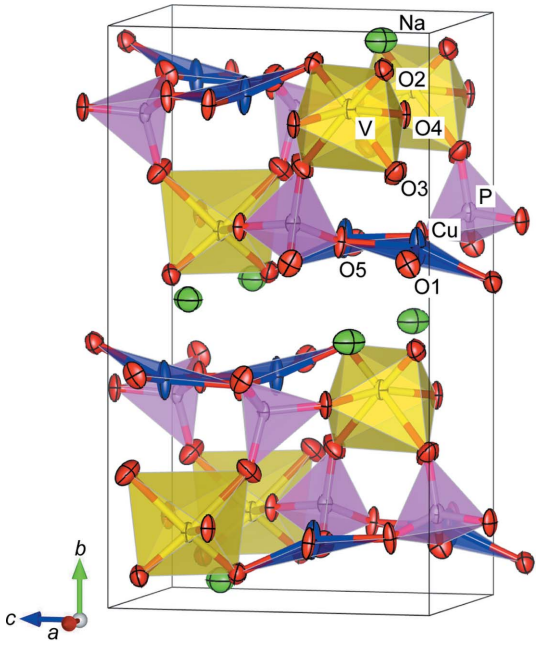

Figure 2
Crystal structure model of $NaCu_2VP_2O_{10}$. Atom colours: Na (green), Cu (blue), V (yellow), P (pink) and O (red). Ellipsoids are set at a 90% probability level.

$2n$ and $h = 2n$ were observed. The [001] zone axis SAED pattern [Fig. 1(*c*)] shows an extinction rule of $h + k = 2n$, which contains both $k = 2n$ and $h = 2n$ in the [100] and [010] zone axis SAED patterns. Such extinction rules indicate the *C* lattice symmetry (*hkl*: $h + k = 2n$) of the orthorhombic system. We then observed the diffraction spots of the 00*l* condition by tilting the specimen to remove the multiple reflections at forbidden reflection positions, which may appear in a crystal structure with screws or grid planes [Fig. 1(*d*)]. The reflections in the 00*l* condition were indexed as $l = 2n$, which represents a twofold screw parallel to the *c* axis (00*l*: $l = 2n$). The extinction rule was identical to that determined from the single-crystal XRD data, which was based on the kinematical theory of diffraction [Figs. S2(*a*)–S2(*c*)]. Analysis of the SAED patterns revealed that the space group of $NaCu_2VP_2O_{10}$ was $C222_1$ and non-centrosymmetric.

Table 1
Crystal data and XRD conditions for $NaCu_2VP_2O_{10}$.

Chemical formula	$NaCu_2VP_2O_{10}$
Space group	$C222_1$ (No. 20)
a (Å)	6.13860 (10)
b (Å)	14.4846 (3)
c (Å)	8.2392 (2)
V (Å)^3	733.58 (3)
Z	4
Dx (Mg m^{-3})	3.84
2θ range	<60.94
Observed reflection	13034
Unique reflection	1110
R_{int}	0.0254
Collection range	$-8 \le h \le 8$ $-20 \le k \le 20$ $-11 \le l \le 11$
R ($F^2 > 3\sigma$)	0.0233
wR (F^2)	0.0762

3.2. Crystal structure determination from XRD data

Single-crystal XRD data obtained for $NaCu_2VP_2O_{10}$ were indexed to an orthorhombic cell, consistent with the SAED patterns. The determined unit-cell dimensions of $NaCu_2VP_2O_{10}$ were *a* = 6.13860 (10) Å, *b* = 14.4846 (3) Å and *c* = 8.2392 (2) Å. The initial structure model was determined using the charge-flipping method. This model represents nine independent sites in the unit cell. The Na site was at the Wyckoff position 4*b* (Na), the Cu site was at 8*c* (Cu), the V site was at 4*b* (V), the P site was at 8*c* (P) and the O sites were at 8*c* (O1–O5). We successfully refined all site-coordination and anisotropic atomic displacement parameters (*U*). The reliability indices were *R* = 2.33% and *wR* = 7.62%. The *U* values were adequate at all sites. The refined crystal structure model is shown in Fig. 2; the crystal data, structural parameters and atomic distances are summarized in Tables 1, 2 and 3, respectively.

The average bond distances of ⟨Na–O⟩, ⟨Cu–O⟩, ⟨V–O⟩ and ⟨P–O⟩ in the crystal structure of $NaCu_2VP_2O_{10}$ were 2.5883, 1.9713, 1.9230 and 1.5343 Å, respectively, which are in good agreement with the bond distances estimated by combinations of the effective ionic radii of the respective ions of 2.58, 1.97, 1.94 and 1.57 Å (Shannon, 1976). The valence of each site was estimated using the bond valence sum (BVS) method, which is used to calculate valence from experimental parameters and bond distances (Brese & O'Keeffe, 1991). The calculated BVS

Table 2
Structural parameters and atomic displacement parameters of $NaCu_2VP_2O_{10}$.

Site	Wyckoff position	g	x	y	z	U_{eq} (Å^2)
Na	4*b*	1	0	0.46651 (11)	1/4	0.0198 (5)
Cu	8*c*	1	0.15209 (6)	0.11957(3)	0.10586 (4)	0.01583 (12)
V	4*b*	1	0	0.86680 (4)	1/4	0.0072 (2)
P	8*c*	1	0.34633 (11)	0.16200 (4)	0.45456 (7)	0.0066 (2)
O1	8*c*	1	0.0438 (4)	0.39928 (14)	0.5749 (2)	0.0119 (5)
O2	8*c*	1	0.1072 (3)	0.06005 (13)	0.8811 (2)	0.0107 (5)
O3	8*c*	1	0.1107 (4)	0.2370 (2)	0.9171 (2)	0.0153 (6)
O4	8*c*	1	0.2228 (3)	0.34868 (13)	0.1330 (2)	0.0104 (5)
O5	8*c*	1	0.3418 (3)	0.37507 (14)	0.8450 (2)	0.0117 (5)

Site	U_{11}	U_{22}	U_{33}	U_{12}	U_{13}	U_{23}
Na	0.0207 (9)	0.0159 (7)	0.0229 (9)	0	0.0051 (8)	0
Cu	0.0051 (2)	0.0363 (2)	0.0061 (2)	0.00172 (14)	0.00042 (13)	0.00126 (13)
V	0.0071 (3)	0.0092 (3)	0.0051 (3)	0	−0.0001 (2)	0
P	0.0046 (3)	0.0099 (3)	0.0054 (3)	−0.0002 (2)	0.0007 (2)	0.0002 (2)
O1	0.0042 (9)	0.0168 (8)	0.0146 (10)	−0.0010 (6)	−0.0016 (7)	−0.0029 (7)
O2	0.0124 (9)	0.0109 (8)	0.0088 (8)	−0.0002 (6)	−0.0005 (7)	0.0009 (7)
O3	0.0162 (10)	0.0167 (9)	0.0131 (10)	−0.0043 (7)	0.0024 (8)	−0.0056 (7)
O4	0.0076 (9)	0.0191 (8)	0.0046 (8)	−0.0006 (7)	−0.0020 (6)	0.0000 (6)
O5	0.0053 (9)	0.0244 (9)	0.0054 (8)	−0.0026 (8)	0.0008 (7)	0.0006 (6)

Table 3
Atomic distances (Å) in $NaCu_2VP_2O_{10}$.

Na–O1	2.861 (2)	(×2)	V–O2	1.649 (2)	(×2)
Na–O1	2.434 (2)	(×2)	V–O3	2.147 (2)	(×2)
Na–O2	2.670 (2)	(×2)	V–O4	1.973 (2)	(×2)
Na–O4	2.388 (2)	(×2)	⟨V–O⟩	1.9230	
⟨Na–O⟩	2.5883				
			P–O1	1.522 (2)	
Cu–O1	1.904 (2)		P–O3	1.516 (3)	
Cu–O2	2.060 (2)		P–O4	1.538 (2)	
Cu–O5	1.949 (2)		P–O5	1.561 (2)	
Cu–O5	1.972 (2)		⟨P–O⟩	1.5343	
⟨Cu–O⟩	1.9713				

values of the Na, Cu, V and P sites were 1.07, 1.84, 5.08 and 4.84, respectively. The average bond distances and BVS values were appropriate, which suggests that the structure analysis was successfully performed. As shown in Fig. 2, Cu ions display characteristic highly anisotropic ellipsoids along the *b* direction. In general, Cu ions in CuO_4 plaquettes prefer the anisotropic displacement perpendicular to the CuO_4 plane because there are no apical oxygen ions (Effenberger, 1990; Smith & Keszler, 1991). Furthermore, $NaCu_2VP_2O_{10}$ has enough space for Cu ions to fluctuate along the *b* direction. The anisotropic ellipsoids of the Cu ions can be interpreted from crystallographic considerations. The Flack parameter, which is an index of the ratio of inversion structure, was determined to be 0.018 (14) (Flack & Bernardinelli, 1999). Therefore, the measured single crystal is regarded as a monodomain crystal with respect to the inversion twin.

3.3. Magnetic susceptibility

Fig. 3 shows the temperature dependence of the magnetic susceptibility measured at 1 T using a single-phase polycrystalline $NaCu_2VP_2O_{10}$ sample. The maximum magnetic susceptibility was observed at ∼60 K and the magnetic susceptibility became close to zero upon further cooling. The Curie–Weiss fitting using $\chi(T) = C/(T - \theta) + \chi_0$ for the high-temperature region (>200 K) represents the Weiss temperature of $\theta = -41.9$ K and Curie constant of $C = 4.04 \times 10^{-1}$ emu K/ mol Cu. The inset in Fig. 3 shows the temperature dependence of $1/\chi$, which represents a straight line owing to Curie paramagnetism in the high-temperature region. Both the effective magnetic moment of $\mu_{eff} = 1.80\mu_B$ and the g factor of 2.07 are decent values for Cu^{2+} ($S = 1/2$) compounds. Fitting for the magnetic susceptibility using the isolated spin dimer model (Bleaney & Bowers, 1952) resulted in failure (Fig. S3). Alternatively, the data can be fitted in the full range using an alternating Heisenberg chain model (Johnston *et al.*, 2000) using the expression $\chi(T) = N_A g^2 \mu_B{}^2/k_B J \times \chi^*(\alpha, T) + C_{imp}/(T - \theta_{imp}) + \chi_0$. Here, N_A, μ_B and k_B are Avogadro number, Bohr magneton and Boltzmann constant, respectively. The exchange parameter J, alternation parameter α (= J'/J), C_{imp}, θ_{imp}, and χ_0 are the fitting parameters. When $\alpha = 0$ and $\alpha = 1$, the function represents the isolated spin dimer and the uniform chain models, respectively. A small impurity Curie–Weiss contribution, which appeared because of magnetic impurities or defects of Cu^{2+} in $NaCu_2VP_2O_{10}$, was observed below ∼5 K. We obtained a Weiss temperature of $\theta_{imp} = -2.38$ K and Curie constant of $C_{imp} = 3.72 \times 10^{-3}$ emu K/ mol Cu, corresponding to 0.99% of nearly free $S = 1/2$ impurities; χ_0 represents the temperature-independent

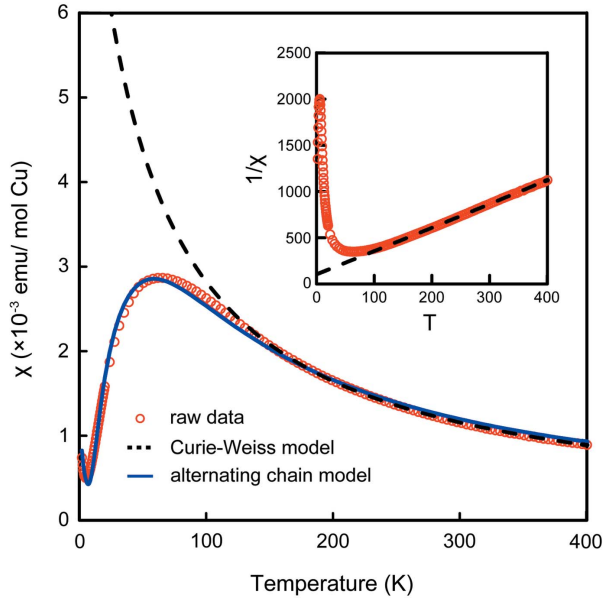

Figure 3
Temperature dependence of the magnetic susceptibility χ of $NaCu_2VP_2O_{10}$. Red open symbols represent raw data. The blue solid and black dashed lines show the fitting curves of the alternating chain and Curie–Weiss models. The inset shows the temperature dependence of $1/\chi$.

term of -2.35×10^{-5} emu/ mol Cu. We obtained $J = 99.3$ K, $\alpha = 0.72$ and a g factor of 2.12 in the $S = 1/2$ alternating chain model. This α value indicates that there are non-negligible interactions between the dimers. Using the relationship $\Delta \simeq J(1-\alpha)^{3/4}(1+\alpha)^{1/4}$, we estimated that the spin gap Δ was 43.4 K. In the thermal analysis, the heat capacity indicated that there were no anomalies below 100 K (Fig. S4). This result suggests that the long-range magnetic order did not evolve and that changes in the magnetic susceptibility were not related to a conventional phase transition. The crystal structure and magnetic susceptibility of $NaCu_2VP_2O_{10}$ indicated that it is a spin-gap system.

4. Discussion

Fig. 4(*a*) shows the crystal structure model of $NaCu_2VP_2O_{10}$. The layered structure consisted of Cu_2O_6 dimers, VO_6 octahedra and PO_4 tetrahedra, which were connected through corner sharing. The Na ions were located between the polyhedral layers. As shown in Figs. 1(*a*) and 1(*c*), the weak diffuse streak scattering along the [010] direction indicates the presence of stacking faults in the layered structure. The Cu_2O_6 dimers were almost parallel to the *ac* plane in each layer. Fig. 4(*b*) depicts the partial structure of one polyhedral layer viewed from the [010] direction. These layers were composed of two-layer units [Figs. 4(*c*) and 4(*d*)]. The two-layer units were related to the twofold screw parallel to the *c* axis, which was constrained by the symmetry of the crystal structure. Each layer unit was connected by corner-sharing VO_6 octahedra and PO_4 tetrahedra. Fig. 4(*c*) displays one of the polyhedral layer units, in which the Cu_2O_6 dimers were connected to two VO_6 octahedra and four PO_4 tetrahedra. The Cu_2O_6 dimers lay in a line approximately parallel to the [101] direction. The PO_4–VO_6–PO_4 polyhedral clusters alternated with Cu_2O_6 dimers to fill the space. In the other polyhedral layer unit, Cu_2O_6 dimers lay in a line almost along the [10 $\bar{1}$] direction [Fig. 4(*d*)].

Fig. 5(*a*) displays the VO_6 octahedron in $NaCu_2VP_2O_{10}$. The VO_6 octahedron showed anisotropic V–O bond distances. In particular, the V–O2 bond distance of 1.649 Å was shorter than that of the other bonds in the VO_6 octahedron. Furthermore, the V–O2 bond distance was not in good agreement with the effective ionic radius of V^{5+} in sixfold coordination $\{r[V^{5+}(6)] + r[O^{2-}(6)]\}$ of 1.94 Å (Shannon, 1976); this bond distance suggests that hybridization occurred between V^{5+} and O^{2-}. Fig. 5(*b*) also shows anisotropic bond distances, which indicate the large off-centre displacement of V ions. The pseudo-Jahn–Teller effect occurs in the d^0 transition-metal octahedra when the empty *d* orbitals of the metal form hybrid orbitals with the filled *p* orbitals of the ligands (Bersuker, 2013; Kunz & Brown, 1995; Halasyamani & Poeppelmeier, 1998; Urushihara *et al.*, 2019). Therefore, V^{5+} ions with a d^0 configuration can display the pseudo-Jahn–Teller effect. It has been reported that in some vanadium oxides, V^{5+} ions in VO_6 octahedra show off-centre displacements in the [110] or [100] direction in simple cubic perovskites (Zavalij & Whittingham, 1999; Halasyamani, 2004). In $NaCu_2VP_2O_{10}$, V^{5+} ions in the VO_6 octahedra also exhibit an off-centre displacement in the [110] direction in the simple cubic perovskite notation. Here, we defined that the direction of the V—O4 bonds is the [001] direction in the simple cubic perovskite. V^{5+} moves toward the edge of O2 ions connected to the Cu_2O_6 dimer, as shown in Fig. 5(*b*). The off-centre displacement would arise from the Coulomb repulsion between the higher valence V^{5+} and P^{5+} ions and pseudo-Jahn–Teller distortion. In potassium vanadium selenite $K(VO_2)_3(SeO_3)_2$, V^{5+} ions also represent an off-centre displacement along the [110] direction in the simple cubic perovskite notation (Harrison *et al.*, 1995). Two of the six V–O bond distances in the VO_6 octahedron are much shorter than those expected based on the effective ionic radius. These shorter V—O bonds could be owing to the off-centre displacement towards the octahedral edge, which is accompanied by hybridization between V^{5+} and O^{2-}, as with $NaCu_2VP_2O_{10}$ compounds.

Fig. 5(*c*) shows the local structure around the Cu_2O_6 dimer. The Cu–O2 bond distance was slightly longer than the other Cu–O

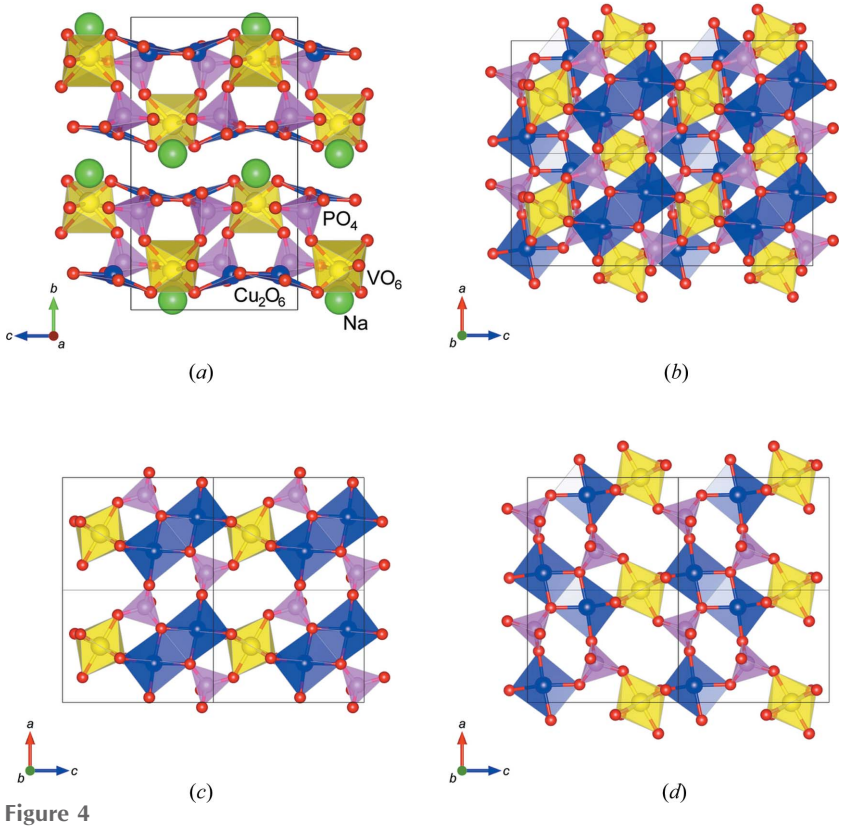

Figure 4
Crystal structure models of (*a*) $NaCu_2VP_2O_{10}$ viewed from the *a* axis, (*b*) the local structure of a single layered structure, (*c*) the upper layer unit and (*d*) the lower layer unit.

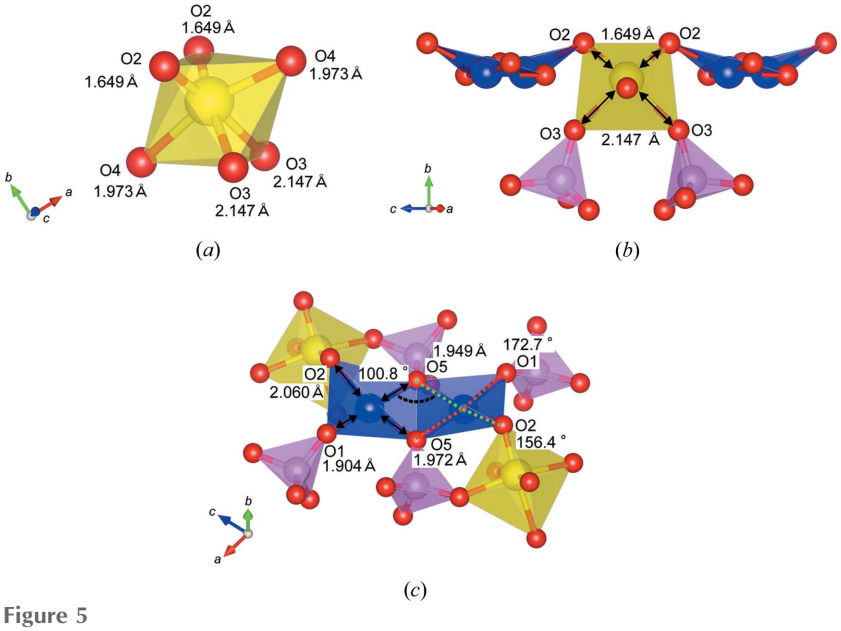

Figure 5
Local structure models of (*a*) a VO_6 octahedron, (*b*) a corner-sharing octahedron and (*c*) a Cu_2O_6 dimer of $NaCu_2VP_2O_{10}$.

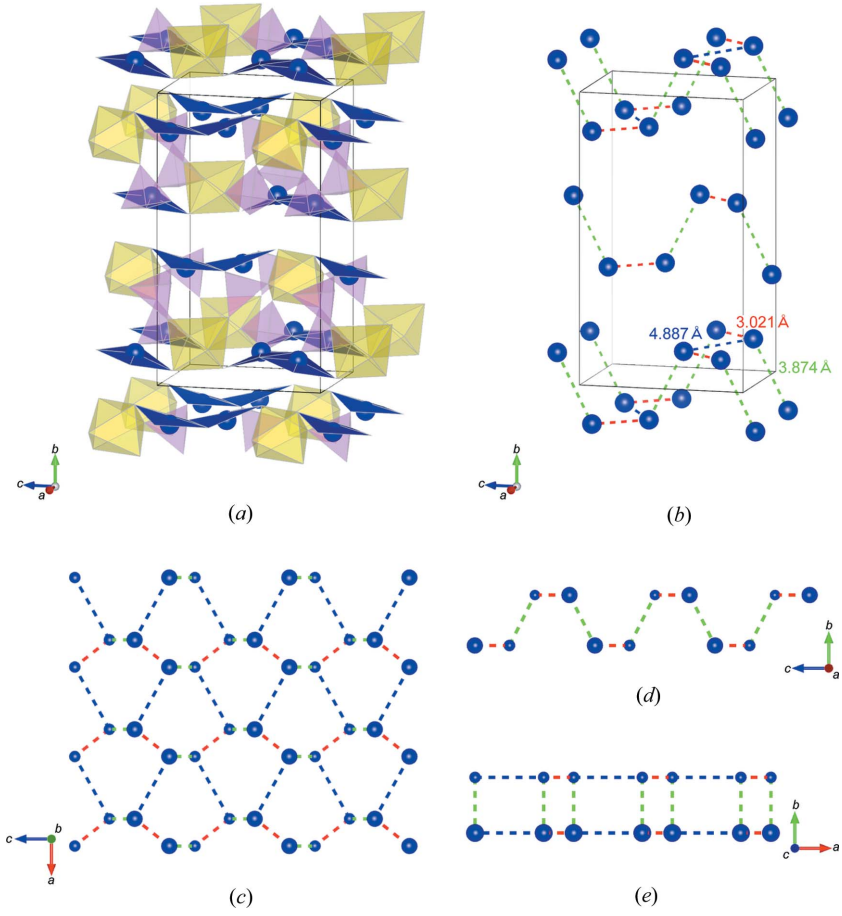

Figure 6
(*a*) Crystal structure model of $NaCu_2VP_2O_{10}$. Na ions are omitted. (*b*) Cu–Cu network and local structures of a single layer of the Cu–Cu network along the (*c*) [010], (*d*) [100] and (*e*) [001] directions. Large and small Cu ions represent the atomic positions at the front and back, respectively. The red, green and blue dashed lines indicate the first-, second- and third-nearest-neighbour Cu–Cu bond distances, respectively.

bond distances. The green and red dashed lines represent ∠O5—Cu—O2 and ∠O5—Cu—O1 bond angles, which were determined to be 156.4° and 172.7°, respectively. The O2 ions are offset from the prescribed position of the planar CuO_4 plaquette. This also suggests that O2 ions strongly connect with V^{5+}, and the bonding state is different from that of other O ions connected to P^{5+}. Thus, $NaCu_2VP_2O_{10}$ is expected to exhibit complicated interactions between Cu ions because of Cu—O—V—O—Cu superexchange interactions.

Fig. 6 shows the Cu–Cu networks, which are arrangements of magnetic ions. The Cu ions form a puckered-layer structure, which has also been observed in other two-dimensional materials such as black phosphorus (Brown & Rundqvist, 1965; Liu *et al.*, 2014). As shown in Figs. 6(*a*) and 6(*b*), the first-nearest-neighbour connection is the Cu pairs in Cu_2O_6 dimers, which have a distance of 3.021 Å. The dimer bridging angle ∠Cu—O5—Cu is 100.8° [Fig. 5(*c*)]; therefore, it is reasonable to suppose that the intradimer exchange interaction is antiferromagnetic (Crawford *et al.*, 1976). The second-nearest-neighbour Cu–Cu connection distance was 3.874 Å and the third-nearest-neighbour connection distance was 4.887 Å. Figs. 6(*c*)–6(*e*) display the single layer Cu–Cu network viewed from different directions. The armchair and zigzag directions are along the *c* and *a* axes, respectively. For a prototypical puckered-layer structure, such as that of black phosphorus, two connections in the layer have the same distances. In contrast, the connections in $NaCu_2VP_2O_{10}$ have different distances, which correspond to the first- and third-nearest-neighbour connections. Therefore, the Cu–Cu network displays a highly distorted puckered-layer structure. As a result, the Cu–Cu network can be regarded as a pseudo-one-dimensional system; that is, the Cu–Cu chains along the armchair direction correlate with each other. Thus, $NaCu_2VP_2O_{10}$ represents a new type of spin dimer compound with a pseudo-one-dimensional system.

5. Conclusions

In this study, we synthesized the spin dimer compound $NaCu_2VP_2O_{10}$. Using selected-area electron diffraction, the space group of $NaCu_2VP_2O_{10}$ was revealed to be $C222_1$. The crystal structure of $NaCu_2VP_2O_{10}$ consisted of a layered structure containing Cu_2O_6 dimers,

VO_6 octahedra and PO_4 tetrahedra. Furthermore, temperature-dependent magnetic susceptibility measurements revealed that $NaCu_2VP_2O_{10}$ has a non-magnetic ground state and spin gap. V^{5+} in the VO_6 octahedra exhibited off-centre distortion caused by the pseudo-Jahn–Teller effect. The hybridization between V and O2 led to complicated interactions via the Cu—O—V—O—Cu path. The crystal structure and magnetic susceptibility results suggest that $NaCu_2VP_2O_{10}$ is a new quantum-spin system owing to dimerized Cu^{2+}.

Acknowledgements

We thank A. Iwasaka for assistance with electron-probe microanalysis and T. Kimura, K. Kimura, M. Tokunaga, A. Miyake and K. Kindo for helpful discussions.

Funding information

This work was partly supported by the Nanotechnology Platform Program (Molecule and Material Synthesis) of the Ministry of Education, Culture, Sports, Science and Technology (MEXT), Japan.

References

Balents, L. (2010). *Nature*, **464**, 199–208.
Bersuker, I. B. (2013). *Chem. Rev.* **113**, 1351–1390.
Bleaney, B. & Bowers, K. D. (1952). *Proc. R. Soc. A*, **214**, 451–465.
Brese, N. E. & O'Keeffe, M. (1991). *Acta Cryst.* B**47**, 192–197.
Brown, A. & Rundqvist, S. (1965). *Acta Cryst.* **19**, 684–685.
Bruker (2015). *APEX3, SAINT* and *SADABS*. Bruker AXS Inc., Madison, Wisconsin, USA.
Crawford, V. H., Richardson, H. W., Wasson, J. R., Hodgson, D. J. & Hatfield, W. E. (1976). *Inorg. Chem.* **15**, 2107–2110.
Effenberger, H. (1990). *Acta Cryst.* C**46**, 691–692.
Flack, H. D. & Bernardinelli, G. (1999). *Acta Cryst.* A**55**, 908–915.
Halasyamani, P. S. (2004). *Chem. Mater.* **16**, 3586–3592.
Halasyamani, P. S. & Poeppelmeier, K. R. (1998). *Chem. Mater.* **10**, 2753–2769.
Harrison, W. T. A., Dussack, L. L. & Jacobson, A. J. (1995). *Acta Cryst.* C**51**, 2473–2476.
Janson, O., Tsirlin, A. A., Sichelschmidt, J., Skourski, Y., Weickert, F. & Rosner, H. (2011). *Phys. Rev. B*, **83**, 094435.
Johnston, D. C., Kremer, R. K., Troyer, M., Wang, X., Klümper, A., Bud'ko, S. L., Panchula, A. F. & Canfield, P. C. (2000). *Phys. Rev. B*, **61**, 9558–9606.
Kageyama, H., Yoshimura, K., Stern, R., Mushnikov, N. V., Onizuka, K., Kato, M., Kosuge, K., Slichter, C. P., Goto, T. & Ueda, Y. (1999). *Phys. Rev. Lett.* **82**, 3168–3171.
Klyushina, E. S., Tiegel, A. C., Fauseweh, B., Islam, A. T. M. N., Park, J. T., Klemke, B., Honecker, A., Uhrig, G. S., Manmana, S. R. & Lake, B. (2016). *Phys. Rev. B*, **93**, 241109.
Kunz, M. & Brown, I. D. (1995). *J. Solid State Chem.* **115**, 395–406.
Lee, P. A. (2008). *Rep. Prog. Phys.* **71**, 012501.
Liu, H., Neal, A. T., Zhu, Z., Luo, Z., Xu, X., Tománek, D. & Ye, P. D. (2014). *ACS Nano*, **8**, 4033–4041.
Momma, K. & Izumi, F. (2011). *J. Appl. Cryst.* **44**, 1272–1276.
Palatinus, L. & Chapuis, G. (2007). *J. Appl. Cryst.* **40**, 786–790.
Petricek, V., Dusek, M. & Palatinus, L. (2014). *Z. Kristallogr.* **229**, 345–352.
Shannon, R. D. (1976). *Acta Cryst.* A**32**, 751–767.
Smith, R. W. & Keszler, D. A. (1991). *J. Solid State Chem.* **93**, 430–435.
Urushihara, D., Asaka, T., Fukuda, K. & Sakurai, H. (2019). *Phys. Rev. B*, **99**, 094104.
Vogt, R. & Müller-Buschbaum, H. (1990). *Z. Anorg. Allg. Chem.* **591**, 167–173.
Zavalij, P. Y. & Whittingham, M. S. (1999). *Acta Cryst.* B**55**, 627–663.